

50

LEVEL

II

12

RADC-TR-81-51

Interim Report

April 1981



AD A101429

HIGH-INTENSITY PULSED PLASMA X-RAY SOURCE FOR MICROLITHOGRAPHY

AVCO Everett Research Laboratory, Inc.

A. Ballantyne

H. Friedman

H. Hyman

APPROVED FOR PUBLIC RELEASE; DISTRIBUTION UNLIMITED

DTIC
ELECTE
JUL 16 1981
S D
H

ROME AIR DEVELOPMENT CENTER
Air Force Systems Command
Griffiss Air Force Base, New York 13441

DTIC FILE COPY

81 7 15 009

This report has been reviewed by the RADC Public Affairs Office (PA) and is releasable to the National Technical Information Service (NTIS). At NTIS it will be releasable to the general public, including foreign nations.

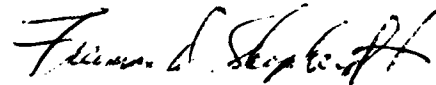
RADC-TR-81-51 has been reviewed and is approved for publication.

APPROVED:



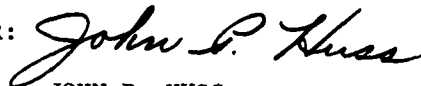
NICHOLAS F. YANNONI
Project Engineer

APPROVED:



FREEMAN D. SHEPHERD, Jr.
Acting Director
Solid State Sciences Division

FOR THE COMMANDER:



JOHN P. HUSS
Acting Chief, Plans Office

If your address has changed or if you wish to be removed from the RADC mailing list, or if the addressee is no longer employed by your organization, please notify RADC (ESE) Hanscom AFB MA 01731. This will assist us in maintaining a current mailing list.

Do not return this copy. Retain or destroy.

UNCLASSIFIED

SECURITY CLASSIFICATION OF THIS PAGE (When Data Entered)

19 REPORT DOCUMENTATION PAGE		READ INSTRUCTIONS BEFORE COMPLETING FORM	
1. REPORT NUMBER RADC-TR-81-51	2. GOVT ACCESSION NO. AD-A20 1429	3. RECIPIENT'S CATALOG NUMBER	
4. TITLE (and Subtitle) HIGH-INTENSITY PULSED PLASMA X-RAY SOURCE FOR MICROLITHOGRAPHY	9	5. TYPE OF REPORT & PERIOD COVERED Interim Report 30 Sep - 31 Dec 80	
		6. PERFORMING ORG. REPORT NUMBER N/A	
7. AUTHOR(s) A. Ballantyne H. Friedman H. Hyman	17) 02	15)	8. CONTRACT OR GRANT NUMBER(s) F19628-80-C-0176
9. PERFORMING ORGANIZATION NAME AND ADDRESS Avco Everett Research Laboratory, Inc. 2385 Revere Beach Parkway Everett MA 02149	16)	10. PROGRAM ELEMENT, PROJECT, TASK AREA & WORK UNIT NUMBER 62704F 27000202	
11. CONTROLLING OFFICE NAME AND ADDRESS Deputy for Electronic Technology (RADC/ESE) Hanscom AFB MA 01731	12) 29	12. REPORT DATE April 1981	
		13. NUMBER OF PAGES 25	
14. MONITORING AGENCY NAME & ADDRESS (if different from Controlling Office) Same		15. SECURITY CLASS. (of this report) UNCLASSIFIED	
		15a. DECLASSIFICATION/DOWNGRADING SCHEDULE N/A	
16. DISTRIBUTION STATEMENT (of this Report) Approved for public release; distribution unlimited.			
17. DISTRIBUTION STATEMENT (of the abstract entered in Block 20, if different from Report) Same			
18. SUPPLEMENTARY NOTES RADC Project Engineer: Mr. Nicholas F. Yannoni (ESE)			
19. KEY WORDS (Continue on reverse side if necessary and identify by block number) x-ray lithography CO ₂ laser design pulsed x-ray source x-ray mask damage laser generated plasma			
20. ABSTRACT (Continue on reverse side if necessary and identify by block number) The objective of the program is to perform a design study for a laser-driven, high-intensity pulsed plasma source for X-ray lithography, including a consideration of the effects of such a source on the X-ray mask structures. During this initial quarterly period, work has begun on the design for the CO ₂ laser driver, as well as on an analysis of the constraints imposed upon the pulsed X-ray source parameters due to thermally-induced stress damage to the mask. (Cont'd)			

UNCLASSIFIED

SECURITY CLASSIFICATION OF THIS PAGE(When Data Entered)

The complete design for the CO₂ laser system must include several subsystems, the most important being the power amplifier module (PAM). During this reporting period, the conceptual design and operating parameters for the PAM have been developed, and tradeoff studies at the interfaces of support systems have been outlined.

Also during this period, a scoping analysis has been performed to examine some of the influences of both x-ray source and mask geometry upon mask thermal stress constraints. Using an analytical model, parametric variation with respect to mask substrate thickness, X-ray wavelength, and X-ray pulselength has been carried out. In addition, some effects of mask configuration have been investigated. These preliminary studies are intended to give an insight into the phenomenology involved in the interaction between intense pulsed X-ray sources and potential mask damage mechanisms. Further analysis along these lines will be carried out over the next several months.

Accession For	
NTIS GRA&I	<input checked="" type="checkbox"/>
DTIC TAB	<input type="checkbox"/>
Unannounced	<input type="checkbox"/>
Justification	
By	
Distribution/	
Availability Codes	
Dist	Avail. and/or Special
A	

UNCLASSIFIED

SECURITY CLASSIFICATION OF THIS PAGE(When Data Entered)

TABLE OF CONTENTS

<u>Section</u>		<u>Page</u>
	List of Illustrations	3
I.	INTRODUCTION	4
II.	CO ₂ LASER DESIGN	7
	A. Introduction	7
	B. CO ₂ Laser Kinetics	7
	C. Gas Mixture Optimization	10
	D. PAM Discharge Parameters	10
III.	ANALYSIS OF X-RAY MASK CONSTRAINTS	19
	A. Problem Scoping	19
	B. Thermal Analysis	22
	C. Preliminary Conclusions	24

LIST OF ILLUSTRATIONS

<u>Figure</u>		<u>Page</u>
1	Schematic of Approach to Source/Mask Design Study	6
2	Simplified Energy Level Diagram for the N ₂ :CO ₂ Molecular Laser System	8
3	Chronology of Laser Kinetics	11
4	Relative Performance of Multipass Laser Extraction	12
5	Kinetics Code Design Map, 1/2 atm, N ₂ :CO ₂ = 1/4:1	14
6	Gain Coefficient Design Map	16
7	Kinetics Operating Point	17
8	Minimum Irradiation Times for Silicon/Gold Masks, Calculated for Different Substrate Thicknesses and Geometries	21
9	Influence of X-Ray Wavelength and Substrate Thickness Upon Minimum Irradiation Times for a 100 Hz X-Ray Source	21
10	Ratio of Conductively Cooled Interface Temperatures (At Typical X-Ray Pulse Durations) to Instantaneous Deposition	25

I. INTRODUCTION

X-ray lithography represents a promising technique for the production of very-large-scale integrated circuits with submicrometer features. In particular, this technique should be useful for ultimately achieving very high resolution, as demonstrated by recent work at MIT, Lincoln Laboratory, (1) which involved the replication of features with linewidths approaching 100 Å. One problem for X-ray lithography, however, is the inherent low brightness of standard e-beam X-ray sources, which necessitates long exposure times and consequently low throughput. The present program addresses the design and development of intense, pulsed plasma X-ray sources together with the effects of such sources on X-ray mask structures.

The standard source in present use is based upon e-beam irradiation of a solid target (usually the anode). Unfortunately, the combination of very low e-beam to X-ray conversion efficiency combined with rather restrictive limits to input e-beam power, imposed by thermal loading of the anode, leads to very low flux levels and consequently very long exposure times. The principal advantages of such sources are that they are inexpensive and readily available. The search for more intense sources has led to a consideration of synchrotron radiation devices for X-ray lithography applications. In many respects synchrotron radiation is very well suited to this application, providing an intense source of soft X-rays in a well-collimated beam (in the plane of the electron orbit). However, the high cost of such machines (estimated at several million dollars) has generally inhibited their use for microlithography.

A fairly recent development, the laser-generated plasma X-ray source, appears capable of offering a compromise solution, providing an intense source of soft X-rays at costs significantly lower than those involved in building synchrotron radiators. For this type of source, a high-power laser beam is focussed onto a target (typically at power densities near 10^{14} W/cm²) producing a high-temperature X-ray emitting plasma. The emission spectrum from the laser-generated plasma generically consists of intense lines in the 1-3 keV range (corresponding to $\lambda \sim 4-12$ Å)

1. Flanders, D.C., "X-Ray Lithography at ~ 100 Å Linewidths, Using X-Ray Masks Fabricated by Shadowing Techniques," 15th Symp. on Electron, Ion, and Photon Beam Technology, Boston (1979).

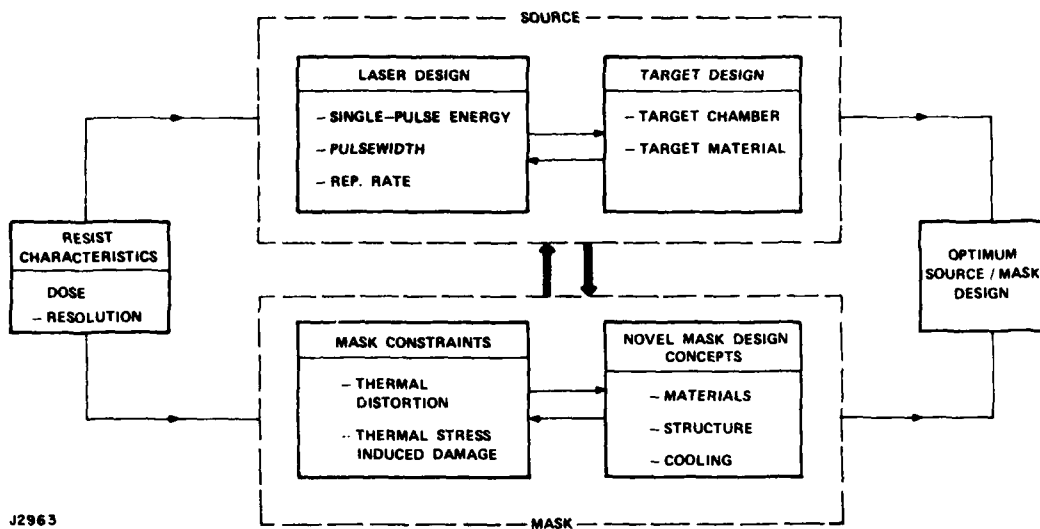
with a continuum that falls off rapidly at higher energies. The hard X-ray component is thus reduced in comparison to e-beam X-ray sources, which should lead to improved contrast. In addition, the source is spatially small, which reduces penumbral blurring effects.

An important characteristic of pulse plasma sources is that each intense X-ray pulse is generally of very short duration (~10 nsec). This leads to rapid heating of the mask elements and can result in thermal distortion and thermal stress induced damage to the mask structures. These effects will play a key role in constraining the laser source design parameters. A thorough understanding of the various damage and distortion mechanisms requires an analysis of the thermal time-evolution of the irradiated mask; to our knowledge this problem has not been previously addressed in detail for intense pulsed sources. Our preliminary analysis of the problem⁽²⁾ has led us to conclude that the most useful approach toward the design of a laser-generated plasma X-ray source is to require low energy per pulse (to minimize mask distortion and damage) and high repetition rate (to maximize throughput). These requirements can best be met by high-power gas lasers (such as CO₂), which can be repetitively pulsed at rates in the range 10-100 pulses/sec. The present design study program is therefore concentrated on a CO₂ laser-driven plasma X-ray source for microlithography applications.

Our preliminary analysis has⁽²⁾ shown that the source design parameters and the mask constraints, arising from potential thermal distortion and/or damage effects, are strongly inter-related. The source/mask combination must therefore be considered in parallel as an integrated system, and extensive parameter trade-offs among the various design elements must be carried out to arrive at an optimum overall design. Our approach to the design study, shown schematically in Figure 1, reflects these considerations.

During the first quarterly period work has begun on the design for the CO₂ laser driver, as well as on an analysis of the constraints imposed upon the pulsed X-ray source parameters due to thermally-induced stress damage to the mask.

2. Proposal for "High Intensity Pulsed Plasma X-ray Source for Microlithography", AERI. (1979).



J2963

Figure 1 Schematic of Approach to Source/Mask Design Study

II. CO₂ LASER DESIGN

A. INTRODUCTION

The complete design for the CO₂ laser system must include several subsystems, the most important being the power amplifier module (PAM). The conceptual definition of the PAM will determine both energy and volumetric efficiency and, hence, the requirements for the gas and electrical power supplies. Concepts such as optical multiplexing, beam transport, and design of the low pressure interface also depend critically on the PAM. In this section the conceptual design and operating parameters for the PAM are developed, and trade-off studies at the interfaces of support systems are outlined.

B. CO₂ LASER KINETICS

Full and detailed descriptions of the kinetics of CO₂ lasers are well known and available in the literature and for brevity will not be repeated here. However, the basic mechanisms are reviewed here to point out the relevant time scales for nanosecond pulse generation and to indicate important trade-offs for support systems.

A simplified energy level diagram for CO₂ is shown in Figure 2. Electrons in the gas are heated by an electrical discharge and collisionally populate the low-lying vibrational levels of N₂ and, to a much weaker extent, the CO₂. Efficient energy transfer occurs between the first vibrational level of N₂ and the 00⁰1 state of the ν_3 (asymmetric stretch) mode of CO₂ in a time scale of

$$\tau_{VV} \cong 100 P(\text{atm}) \text{ ns}$$

where P = pressure of the PAM lasing medium. Thus, once the upper lasing level of CO₂ and the energy reservoir (the $\nu = 1$ level of N₂) come into equilibrium and a nanosecond pulse of CO₂ energy is extracted, no more energy can be extracted from the reservoir in times short compared to 100 ns (for near atmospheric pressure lasers). For additional energy extraction and high efficiency operation, the optical pulse must be delayed and repassed through the PAM. This technique is known as optical multiplexing and can increase the total energy extracted by

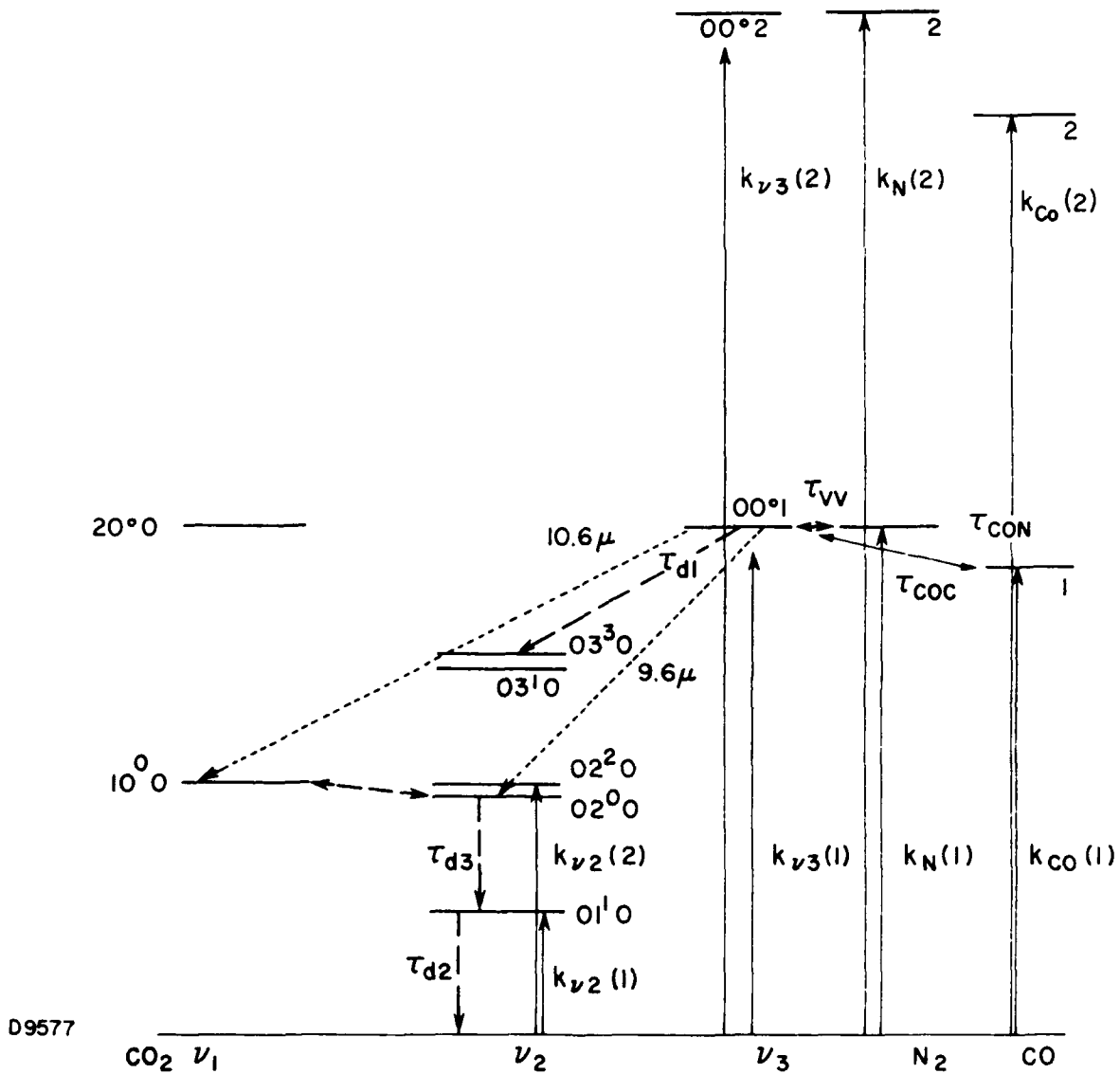


Figure 2 Simplified Energy Level Diagram for the $N_2:CO_2$ Molecular Laser System

almost a factor of 3. The trade-off between the optical and mechanical complexity and the increase in laser performance will be evaluated.

An additional observation is that the energy extraction is independent of pulse duration for pulse lengths $\lesssim 100$ ns. At the opposite extreme of pulse duration, i.e. $\lesssim 3$ ns and/or cavity pressure, i.e., $\lesssim 1/2$ atm, not all of the available energy can be extracted due to inability of the finely divided rotational sublevels of the lasing transition to transfer their energy. An approximate relationship for the fraction of energy extraction is

$$E/E_{\text{MAX}} \cong 1 - \exp \left[-nP (\tau_p/3) \right]$$

where

n = number of rotational transitions used in the extracting pulse

τ_p = pulse length in nanoseconds

P = cavity pressure in atmospheres.

Hence, at one atmosphere and one rotational transition, a 5 ns pulse can extract over 80% of the stored energy. Furthermore, by dropping the cavity pressure to 1/2 atm, which has advantages with regard to the pulsed power and pressure interface systems, a single transition pulse of 10 ns duration will also extract over 80%.

The next time scale of interest, that required to pump the vibrational nitrogen manifold, is a function of the electron density and temperature, nitrogen fraction, and cavity pressure. The time scale for deactivation of the upper laser level (collisional deactivation to the ν_2 mode) is several microseconds for atmospheric pressures, and hence the possibility exists to pump the laser mixture slowly (several microseconds at sub-atmospheric pressures) thereby easing the requirements on the pulse power system. Optimization of the pumping conditions and trade-offs with the pulsed power systems will be performed.

The final time scale of interest is concerned with the deactivation of the lower laser level. Since the lower laser levels of both the 9.6 and 10.6 μ bands are closely coupled, lasing on either band results in a population of the 02°0 level of the ν_2 mode. Thermalization of the ν_2 mode occurs rapidly,

within a few tens of nanoseconds, so that the first vibrational level of the ν_2 mode acts as an energy sink for the lower laser level. Since very large fractional concentrations of a gaseous deactivator, e.g., He or H₂, are needed to equilibrate the first vibrational level of the ν_2 mode with the ground state, i.e., thermalization, in short times, there is no need for and little benefit to their use.

In summary, the chronological sequence of the short pulse CO₂ laser system is depicted in Figure 3. The discharge heated electrons pump the N₂ and CO₂ vibrational manifold in several microseconds. A 10 ns pulse extracts energy from the PAM leaving the laser medium (in the fully saturated case) with equal upper and lower laser level populations. In a few tens of nanoseconds, the bulk of the lower laser level population resides in the lowest level of the ν_2 mode leaving the lower laser level relatively empty. After a delay of a few hundreds of nanoseconds, the N₂ reservoir repopulates the upper laser level and another pulse can be amplified. This process can continue until the N₂ reservoir becomes depleted or the lower laser level fills up. The delays in the optical pulses are removed and all pulses are combined onto the target, simultaneously.

C. GAS MIXTURE OPTIMIZATION

The ratio of N₂ to CO₂ in the PAM gas mixture can be optimized according to the operating conditions which are chosen. For example, if the ratio of N₂ to CO₂ is very high, the N₂ vibrational manifold will be efficiently pumped, but since the number of CO₂ molecules is reduced, little laser energy can be extracted in a pulse, and many passes, each separated by hundreds of nanoseconds, will be required. For low values of this ratio, large pulse energies could be extracted on a single pass, but the pumping efficiency is low. The optimum value of N₂ to CO₂ is illustrated in Figure 4. For 1 or 2 pulses, the optimum performance occurs for an N₂ fraction of $\psi_N \approx 0.25$. Also, the maximum performance increase is a factor ~ 2.5 . There are other factors which limit the number of passes to $\sim 4-5$, e.g., optics complexity and laser medium homogeneity, so that the performance increase is < 2 . Preliminary estimates from a trade-off between increased laser size and optical multiplexing for the same output energy tend to favor larger lasers and one single optical pass through the gain medium.

D. PAM DISCHARGE PARAMETERS

The three discharge parameters which specify the kinetic operation of the PAM are the cavity pressure, the electron density, and the discharge electric field, which in essence controls the electron temperature. The range of acceptable cavity pressures is limited to $1/2 < P < 1$ atm for reasons of

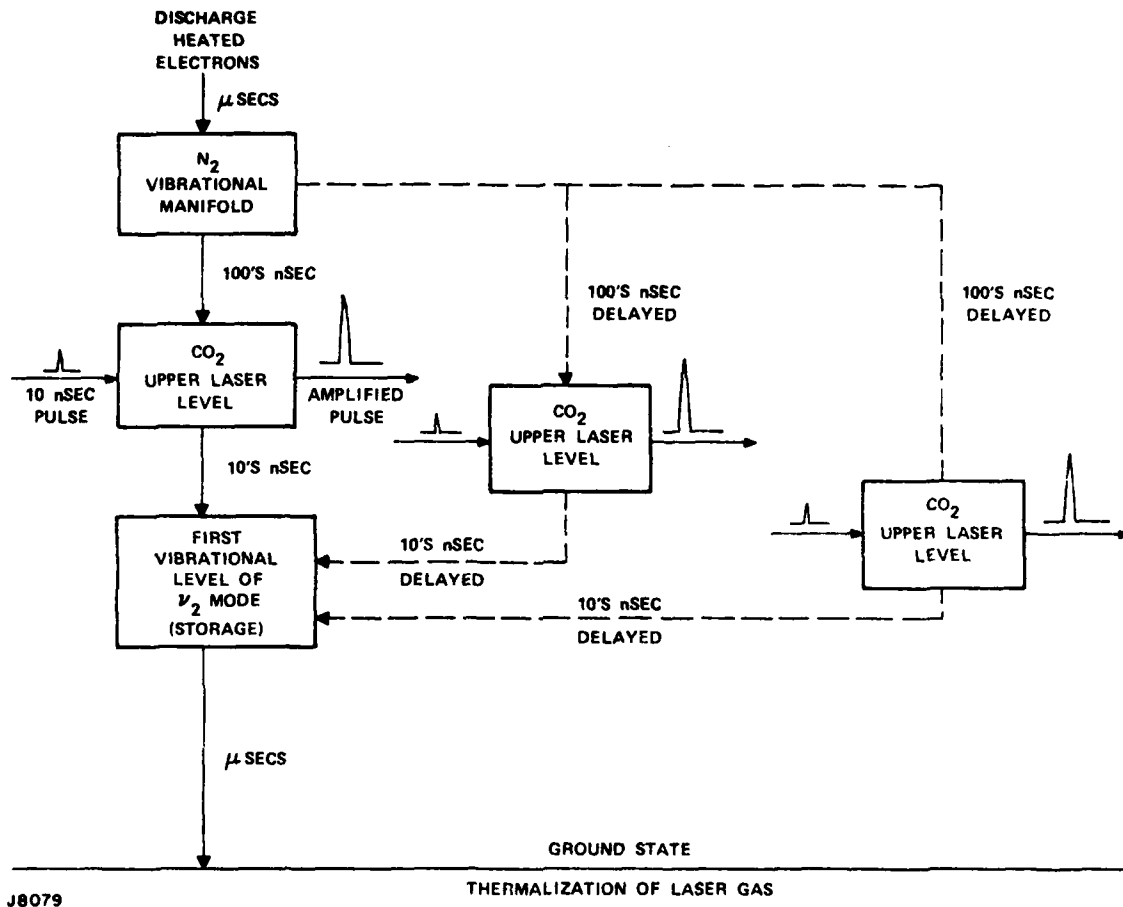
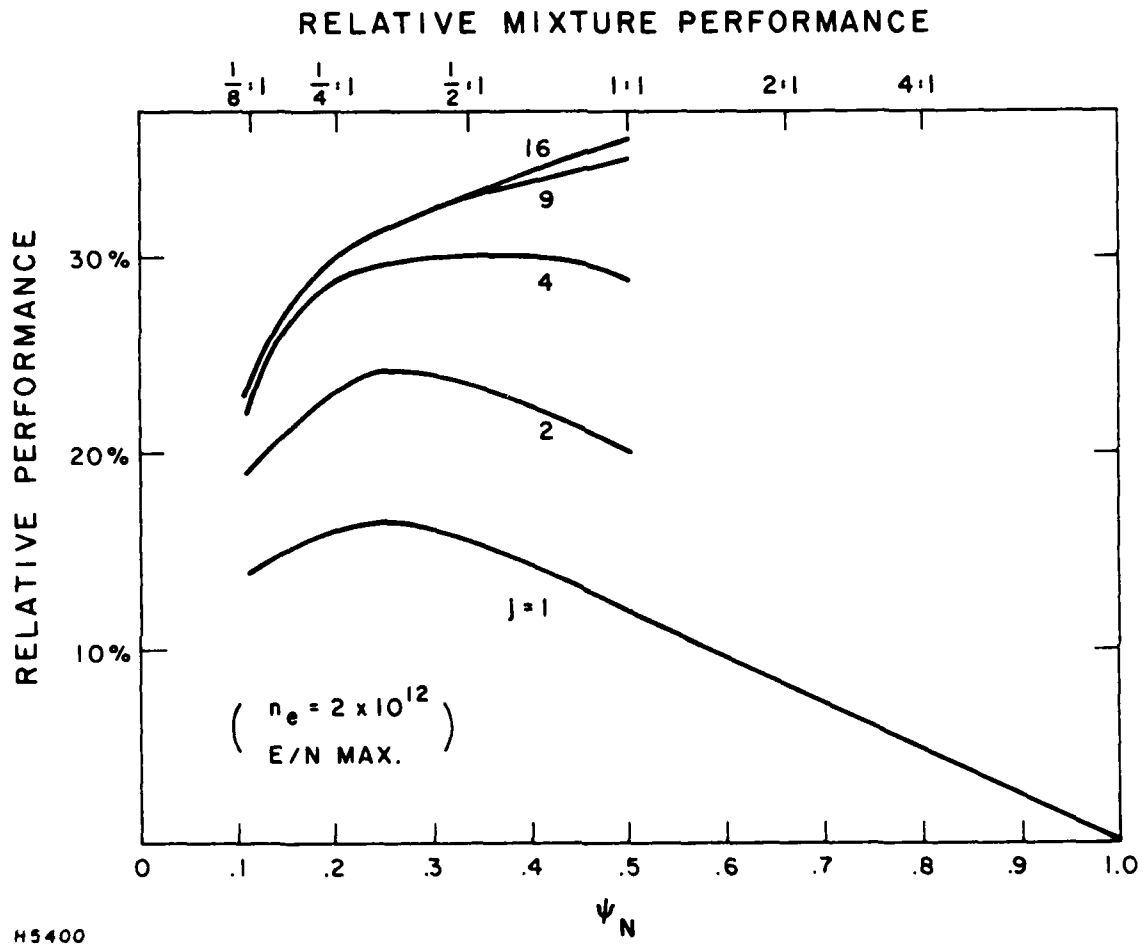


Figure 3 Chronology of Laser Kinetics



H5400

Figure 4 Relative Performance of Multipass Laser Extraction

efficient energy extraction in 10 ns pulses at the low end and very short electrical pumping times on the high end. The discharge electric field (normalized to the neutral particle density) is also limited to a range of $4 \times 10^{-16} < E/N < 5 \times 10^{-16}$ V-cm² as confirmed by computer code studies. The remaining parameter, the electron density, controls the pumping rates and can vary between $10^{12} < n_e < 10^{13}$ cm⁻³. At the low end, although the efficiency is high, the volumetric energy loading, and hence output energy density is low, thereby requiring a large volume of laser gas. At the high end of the range, the input energy loading is high, but the pumping time scales are short in order to favorably compete with loss mechanisms such as electron pumping to unwanted levels and electron deactivation of the upper laser level. A convenient display of this information is shown in Figure 5 which is a result of a detailed computer code description of the pumping kinetics. For electron densities between 10^{12} and 10^{13} cm⁻³, the efficiency of pumping the upper laser level is plotted as a function of the input energy loading. The upper state pumping efficiency,

$$\frac{g_0 E_{SAT}}{Q} = \frac{(\sigma \Delta N) (h\nu/\sigma)}{Q} = \frac{\Delta N h\nu}{Q}$$

where

Q = input energy density (J/l)

σ = stimulated emission cross section

ΔN = population inversion density

= upper-lower laser level density

$h\nu$ = laser photon energy

represents the fraction of input energy available for laser extraction. For a well saturated laser amplifier, the output energy density is $\alpha g_0 E_{SAT}$ where α is 0.5 for 1 band and 2/3 for 2 band extraction. Hence, for the 1/4:1 mixture plotted in Figure 5, the intrinsic laser efficiency (output energy/energy absorbed in the gas) for one pulse is ~7.5 - 10% depending upon whether one or two vibrational bands are extracted. It is important to notice that all quantities are normalized to pressure, i.e., n_e/P , $E/N \sim E/P$, Q/P , $g_0 E_{SAT}/Q = g_0 (E_{SAT}/P)/(Q/P)$ because in a N₂:CO₂ laser system, where only binary collisions are important, all quantities scale with pressure. The impact of the design map of Figure 5 is that there is a trade-off

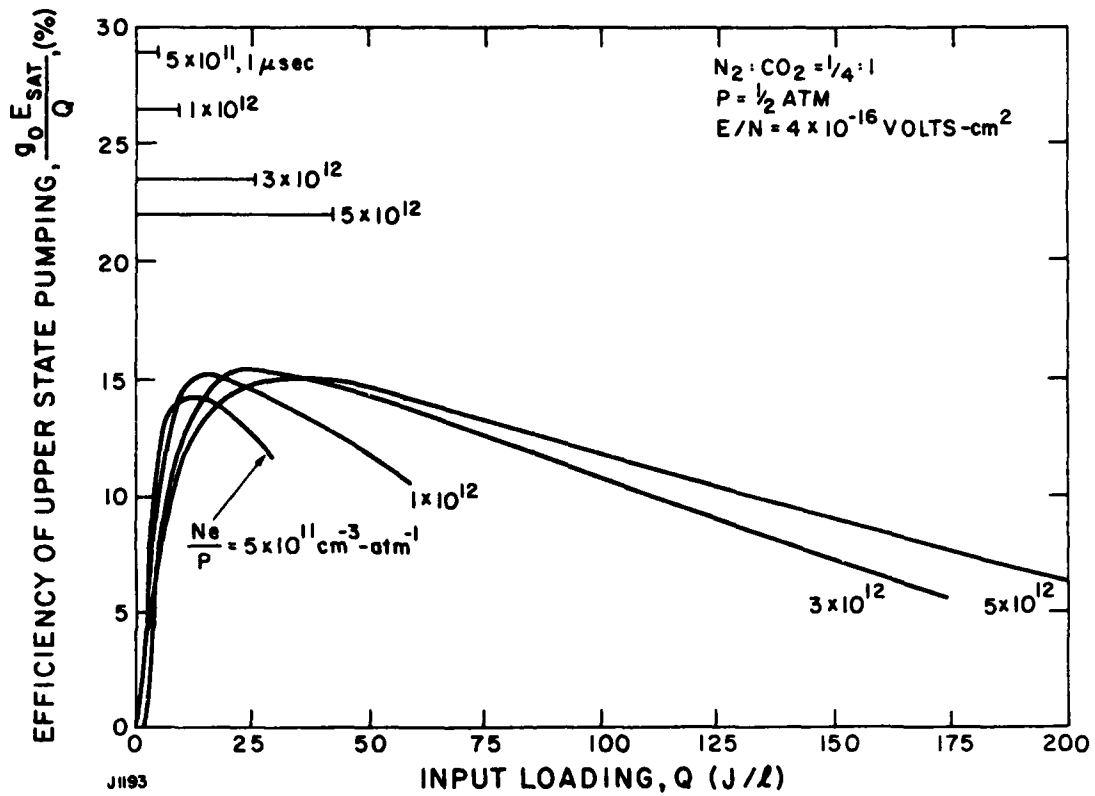


Figure 5 Kinetics Code Design Map, 1/2 atm, N₂:CO₂ = 1/4:1

between the pumping efficiency and the input energy loading, or equivalently between the pumping efficiency and the output energy density. For a fixed electron density, peak efficiency occurs at low output energy density, i.e., large laser volumes and the efficiency falls off with increased outputs, hence, the trade-off between efficiency and PAM size. Another trade-off which is of crucial importance to the design of the pulsed power system is indicated by the horizontal lines at the top left corner of the plot, which give the time scale in $1 \mu\text{s-atm}$ increments. Therefore, the $n_e/P = 10 \times 10^{12} \text{ cm}^{-3}$ curve can accommodate large input energy loadings at only a small decrease from peak efficiency, i.e., 200 J/l-atm input at $\sim 12\%$ efficiency, corresponding to $12\text{-}16 \text{ J/l-atm}$ output (1 or 2 band extraction); the pump time to achieve these conditions is $\sim 1.2 \mu\text{s-atm}$. The detailed trade-off between pulsed power efficiency and duration of the pumping pulse remains to be done, but in general, high-power, repetitively pulsed systems become complicated below pulse durations of a microsecond. At a reduced electron density, i.e., $n_e/P = 1 \times 10^{12} \text{ cm}^3$, the same 12% efficiency point occurs at 60 J/l-atm with a pump time of $\sim 3.3 \mu\text{s-atm}$. In this case the output energy density is only $3.6 - 4.8 \text{ J/l-atm}$, and hence the laser is much larger.

There is an additional constraint aside from those imposed by PAM volume, efficiency, and pump time, and that has to do with the value of small-signal gain and the maximum gain standoff permissible before the onset of parasitic oscillations. To see the effect of gain on the kinetics code design map of Figure 5, the small signal gain, g_0 , is plotted in Figure 6, according to the relationship:

$$g_0 = \frac{Q/P}{E_{\text{SAT}}/P} \times (\text{efficiency of upper state pumping})$$

where $E_{\text{SAT}}/P \approx 0.2 \text{ J/cm}^2\text{-atm}$ over a wide range of input energy loadings. Hence, the locus of constant g_0 are hyperbolae when plotted on the axes of Q/P and upper state pumping efficiency. If one wishes to operate at high efficiency and high input energy density, then the small-signal gain will be high and the PAM dimensions will be restricted by the onset of parasitics.

The information displayed in Figures 5 and 6, although useful for a conceptual understanding of some of the design considerations for CO_2 lasers, may not be in the most straightforward way to choose an operating point. The same information is plotted in a different format in Figure 7. Here the photon energy density in the PAM gain medium is plotted as a function of pump time for various electron densities. All quantities are normalized to pressure as before, with the exception of the

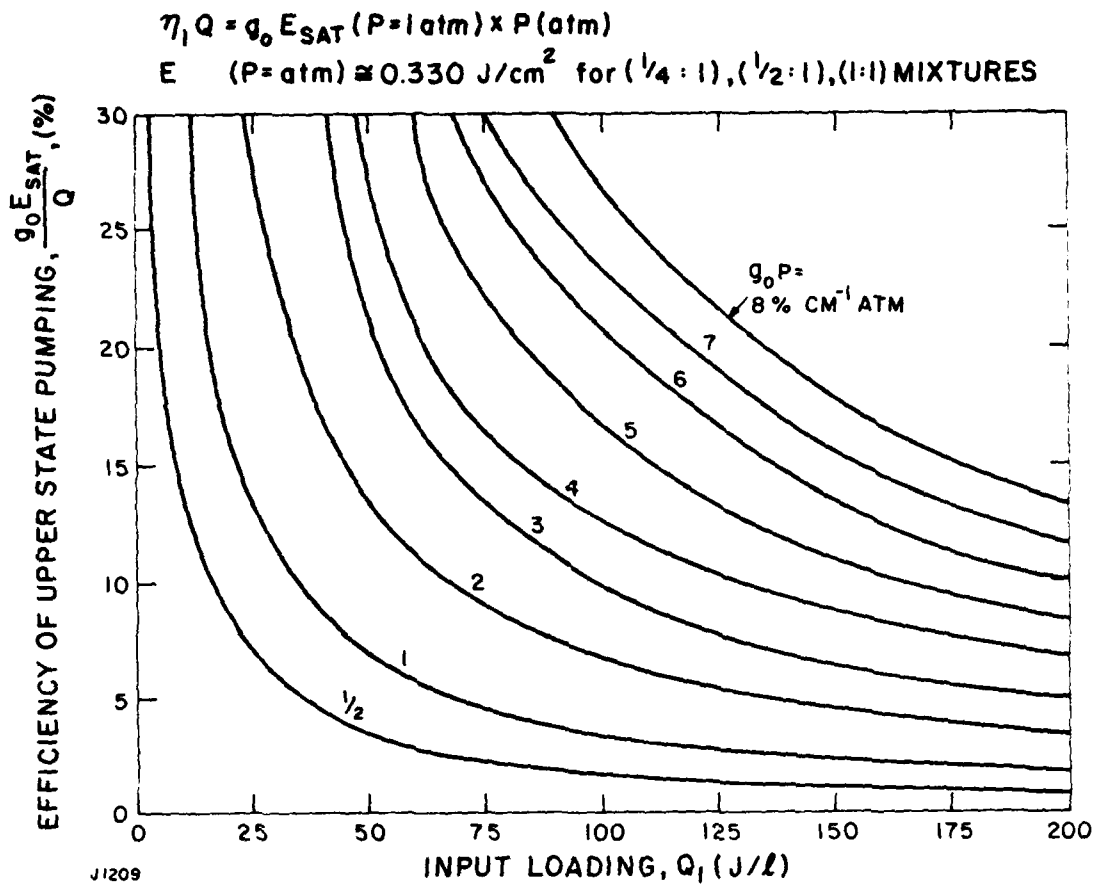
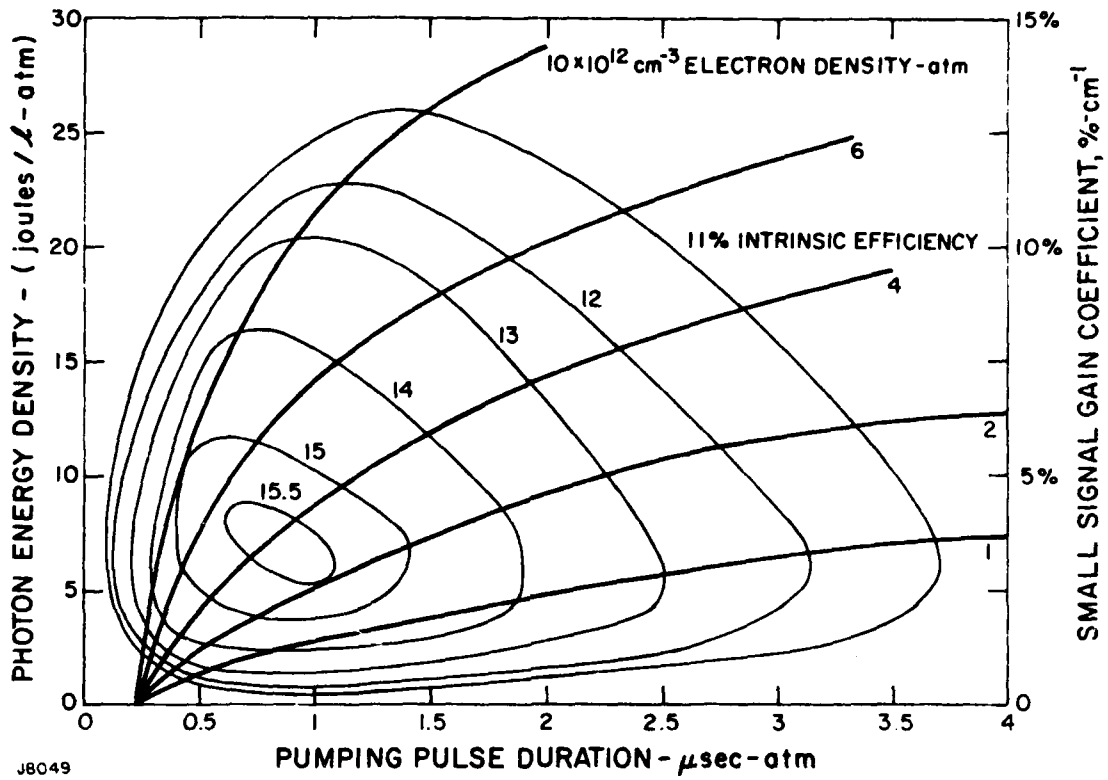


Figure 6 Gain Coefficient Design Map



J8049

Figure 7 Kinetics Operating Point

small signal gain, which to first order is independent of pressure. The contours of constant efficiency are indicated with light lines and it is clear that the kinetic performance of the laser system is not a strong function of efficiency. In fact, if operating at the peak efficiency results in a short pumping pulse, the inefficiency of the pulsed power system could easily negate any gains in intrinsic efficiency.

Several factors influence the preliminary choice of operating point as shown in Figure 7. The primary factor is the maximum gain stand off before the onset of parasitics. In theory, the product, g_0L , is crucial since for a single pass amplifier the maximum g_0L product attainable, with careful attenuation paid to spurious reflections, is $\sim 12^*$. However, it is advantageous to achieve the gain length product by a lower value of g_0 rather than by decreasing the length and increasing the gain. The reason for this choice is that a short gain length would require a larger cross section to make up the required volume. Large cross sections are incompatible with high pulse repetition rates and would require large input (laser) pulse energies to saturate the PAM gain medium. Hence, keeping the gain coefficient low and the stored energy density high restricts one to operate at the low pulse duration corner of the map. Other systems considerations will provide tradeoffs for the operating point, and these remain to be investigated.

The preceding work represents the basis for choosing the kinetic operating point for the PAM, and hence the general requirements for the gas and flow handling, pulse power, optical, and pressure interface systems. Subsequent work will define these systems in detail.

*A (g_0L) product of 14 has been achieved for several microseconds (T. Cronburg and M. Sirchis, AERL private communication).

III. ANALYSIS OF X-RAY MASK CONSTRAINTS

A. PROBLEM SCOPING

The objective of this preliminary analysis is to obtain a qualitative picture of the parametric variation of mask constraints. The primary area of concern has been that of thermally induced stress damage to the mask. In prior work(2) it had been established that pulsed X-ray sources can induce single pulse failure of the mask arising out of differential thermal expansion at the substrate/absorber interface. On a longer timescale, multipulse irradiation becomes dominated by convective cooling requirements if stress damage is to be avoided. This initial work indicated areas of concern and the relevant phenomenology that should be investigated to evaluate the potential of intense pulsed X-ray sources for microlithography.

The initial simplified analysis has been extended over a wider range of parameters in order to facilitate a better understanding of the problems arising out of pulsed irradiation of generic mask structures. The simple analysis results in an expression for thermal stress limiting irradiation times under an initial exponential temperature profile through the absorber and substrate materials given by

$$t_D = \frac{J_{TOTAL} \cdot \tau_{CONV}}{J_{D,MAX} \cdot X} \ln \left[\frac{1}{1 - \frac{X}{F_X} K} \right]$$

where t_D is the total minimum required irradiation time for a given pulse fluence ($J_{D,MAX} \cdot X$), where $J_{D,MAX}$ is the single pulse damage fluence and X the fraction of the pulse fluence to the damage fluence. J_{TOTAL} is the total required dosage. τ_{CONV} is the convective cooling time for the mask. The parameter K is given by

$$K = \frac{\Delta T_{P,MAX}}{\Delta T_{MAX}} \cdot \left(\frac{\Delta T_E}{\Delta T_P} \right)$$

where

$\Delta T_{P,MAX}$ is the peak interface temperature difference for stress failure.

ΔT_{MAX} is the equilibrated temperature rise in the mask for stress failure.

$(\Delta T_E/\Delta T_P)$ is the ratio of the equilibrated temperature rise to the pulsed interface temperature difference.

The relevant parameters of interest in evaluation of this irradiation time, are the mask thickness (which defines the convective cooling time), the X-ray wavelength (which defines absorption depths and $J_{D,MAX}$), and mask geometry (which defines energy absorption and temperature rises). Some typical results of this analysis are shown in Figure 8, for irradiation at 4 Å wavelength. The conditions for these calculations were a gold absorber/silicon substrate mask, with an assumed failure condition given by an axial stress of 2×10^8 N/m² (corresponding to the yield stress of single crystal gold⁽³⁾) and a dosage requirement of 1 J/cm² (approximating a PMMA resist). As can be seen, the thicker the substrate, the longer the irradiation time. This is primarily the result of an increasing convective cooling time for the mask, as

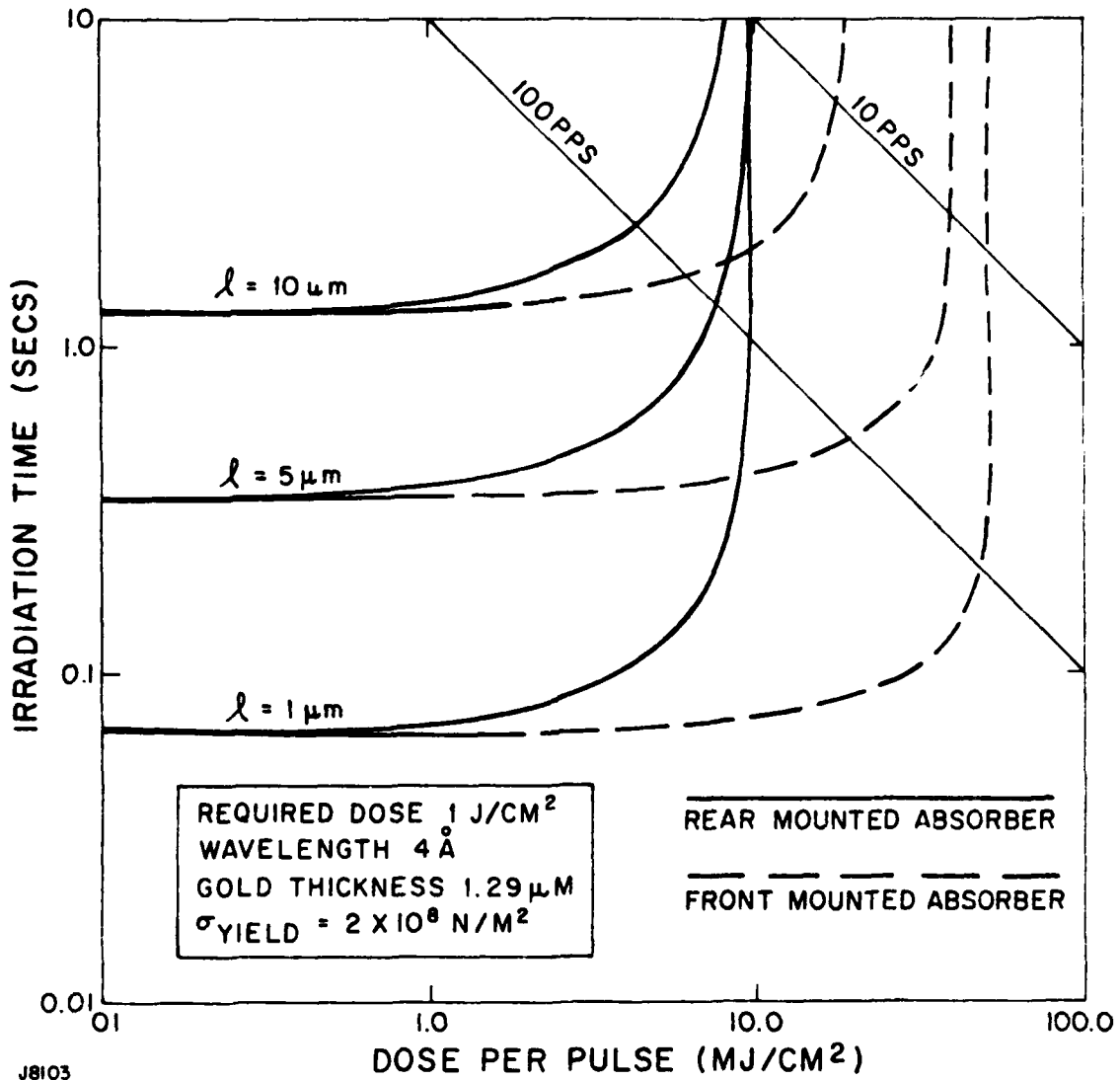
$$\tau_{CONV} \approx \frac{(\rho c) \ell}{h}$$

ρc being the volumetric specific heat, ℓ the mask thickness and h the heat transfer coefficient.

With increasing pulse dosage the convective cooling dominates the total irradiation time, sharply limiting the pulse fluence and rapidly increasing the required irradiation times. Cross plotted on the figure are 10 and 100 Hz irradiation times, indicating the minimum irradiation times required for possible pulsed laser/X-ray regimes.

It can be seen in Figure 8, that there is considerable difference in irradiation times for the two mask geometries considered. In one case the standard configuration is used; i.e., gold absorber between substrate and resist (rear mounted). In the other the gold is mounted above the substrate (front mounted); this is generally not used in existing X-ray lithography as

3. Beams, J.W., "Structure and Properties of Thin Films", p. 183. Wiley, New York (1959)



J8103

Figure 8 Minimum Irradiation Times for Silicon/Gold Masks, Calculated for Different Substrate Thicknesses and Geometries

penumbral blurring is increased as a result of greater absorber-resist separation. However under intense laser generated plasma conditions, the increased source-mask separation may allow such configuration changes. The front mounted absorber allows for a higher pulsed dosage, as the interface temperature rise is smaller than for a corresponding rear mounted absorber. In the limit of high repetition rate, the two cases become asymptotic.

Figure 9 illustrates the effect of X-ray wavelength upon irradiation times for a 100 Hz source, and a rear mounted absorber. All the curves correspond to a fixed contrast ratio ($=e^{h/\lambda a}$, h = absorber thickness, λ_a = absorption depth). As can be seen, the shorter the X-ray wavelength, the shorter the irradiation time. At longer wavelengths ($\sim 20 \text{ \AA}$) where absorption depths are small and energy absorption becomes significant in the substrate, the effect of mechanical stiffness requirements upon allowable substrate thickness can be seen to result in a rapid increase in irradiation times.

B. THERMAL ANALYSIS

The prior analysis is based on an idealized instantaneous absorption of radiation, giving exponential temperature profiles through the absorber and substrate. In reality, the typical absorber thicknesses are comparable to the thermal relaxation length for typical X-ray pulse durations, indicating that smoothing of the temperature profile across the interface is possible. A thermal analysis of this problem has been obtained. For a thin absorber layer mounted on a semi-infinite substrate, the interface temperature can be calculated for an exponential deposition of energy to be

$$\theta_{\text{INTERFACE}} = \left(\frac{J_D}{\rho c \lambda}\right) \left[\left(\frac{e^\beta - 1}{\beta}\right) - \frac{e^\beta}{2\beta} [\text{erfc}(-\sqrt{\beta}) + \frac{1}{c} \text{erfc}(2\gamma - \sqrt{\beta}) - \text{erfc}(\gamma - \sqrt{\beta}) + \text{erfc}(\gamma + \beta)] + \frac{h}{\lambda c \beta} \text{erfc}(\gamma) - \frac{1}{2\beta} \left[\left(\frac{2h}{\lambda} - 1\right) \text{erfc}(2\beta) - 1 \right] + \frac{1}{\sqrt{\beta \pi}} \left[1 + e^{-4\gamma^2} - \frac{2}{c} e^{-\gamma^2} \right] \right]$$

for $\beta = \alpha \tau_x / \lambda^2$

$$\gamma = \frac{h}{2\sqrt{\alpha \tau_x}}$$

and $c = \exp(h/\lambda)$ (\approx the contrast ratio)

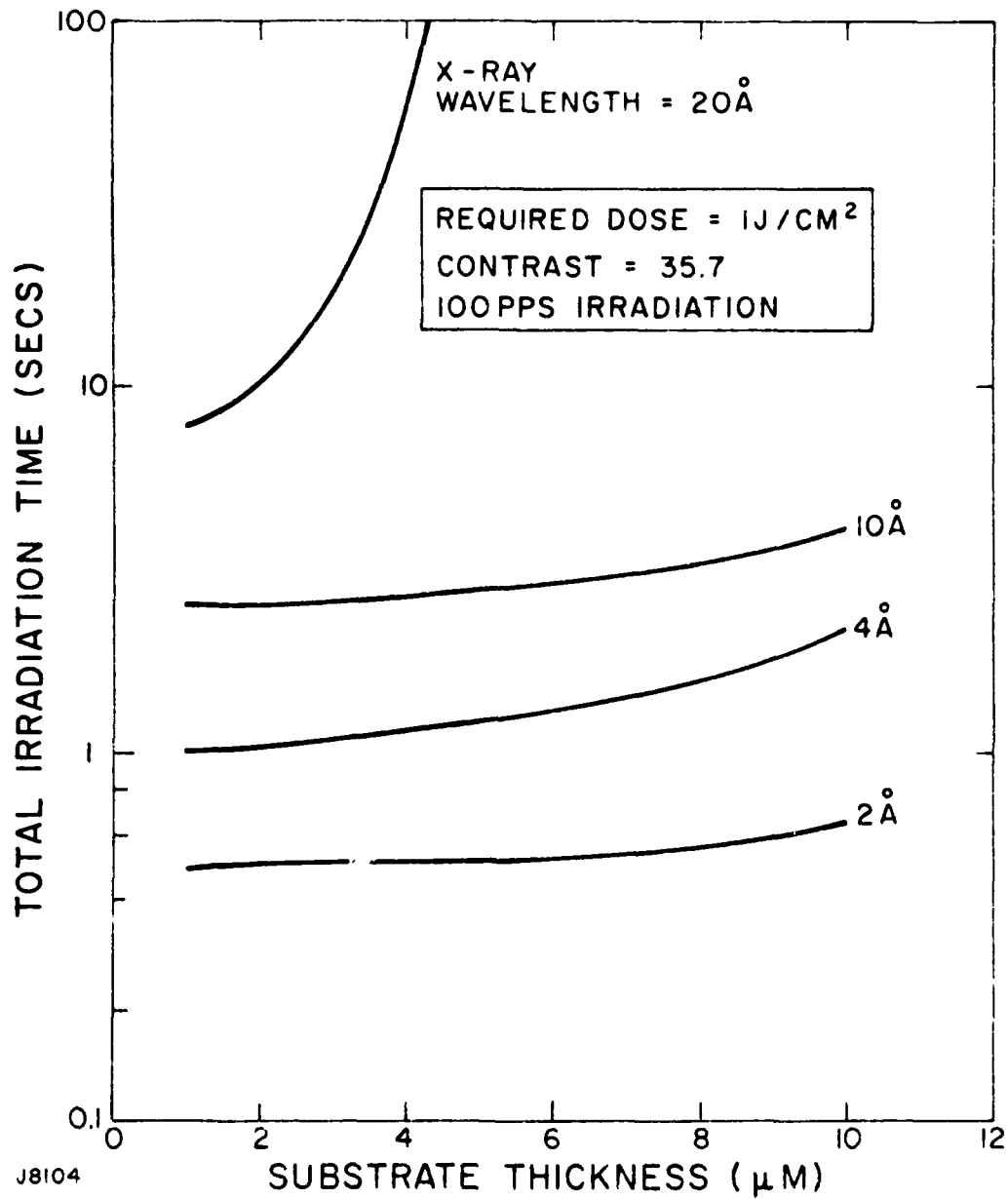


Figure 9 Influence of X-Ray Wavelength and Substrate Thickness Upon Minimum Irradiation Times for a 100 Hz X-Ray Source

where τ_x is the X-ray pulse duration

α is the thermal diffusivity of the mask ($\approx 1.0 \text{ cm}^2/\text{sec}$)

h is the absorber thickness

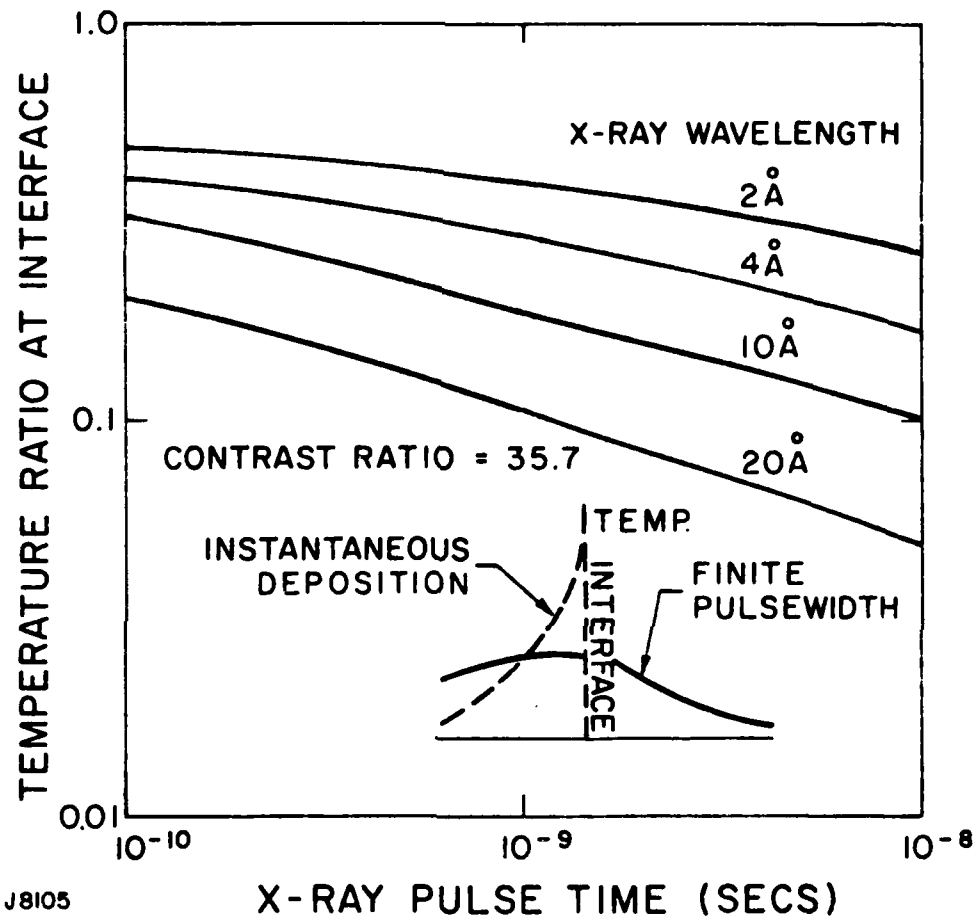
λ is the absorption depth

This analysis assumes constant thermal properties throughout and no thermal resistance across the interface. For short pulse duration the semi-infinite substrate assumption is a good approximation. The constant thermal property also appears a reasonable approximation to the limit of accuracy of interest. Figure 10 illustrates the conductive cooling at the interface under typical conditions of interest. For pulse durations between 0.1 and 10 ns it can be seen that significantly lower temperatures are obtained at the interface, as compared with that for instantaneous deposition.

C. PRELIMINARY CONCLUSIONS

The scoping analysis has given insight into mask constraints via a set of preliminary parametric evaluations. These include:

- 1) The mask geometry affects the single-pulse fluence damage threshold and also results in differences in required irradiation time.
- 2) Under convective cooling conditions, substrate thickness has some effect upon irradiation time, at representative operational pulse repetition frequencies.
- 3) X-ray wavelength has a strong influence upon the required irradiation times, with shorter wavelengths being more attractive for implementation of pulsed X-ray sources.
- 4) Significant conduction of energy across the mask interface appears to occur for representative pulse durations. This would enhance the possible single-pulse damage criteria above the estimates obtained under idealized instantaneous deposition.



J8105

Figure 10 Ratio of Conductively Cooled Interface Temperatures (At Typical X-Ray Pulse Durations) to Instantaneous Deposition



MISSION
of
Rome Air Development Center

RADC plans and executes research, development, test and selected acquisition programs in support of Command, Control Communications and Intelligence (C³I) activities. Technical and engineering support within areas of technical competence is provided to ESD Program Offices (POs) and other ESD elements. The principal technical mission areas are communications, electromagnetic guidance and control, surveillance of ground and aerospace objects, intelligence data collection and handling, information system technology, ionospheric propagation, solid state sciences, microwave physics and electronic reliability, maintainability and compatibility.